Measurement of high carrier mobility in graphene in an aqueous electrolyte environment

Morgan A. Brown,[1] Michael S. Crosser,[2] Matthew R. Leyden,[3] Yabing Qi,[3] and Ethan D. Minot[1,*]

[1]*Department of Physics, Oregon State University, Corvallis, Oregon 97331, United States*

[2]*Department of Physics, Linfield College, McMinnville, Oregon 97128, United States*

[3]*Energy Materials and Surface Sciences Unit (EMSS), Okinawa Institute of Science and Technology Graduate University (OIST), 1919-1 Tancha, Onna-son, Okinawa 904-0495, Japan*

* Author to whom correspondence should be addressed. Electronic mail: ethan.minot@oregonstate.edu

Abstract

Graphene is a promising material for applications in aqueous electrolyte environments. To explore the impact of such environments on graphene's electrical properties, we performed Hall bar measurements on electrolyte-gated graphene. Assuming a Drude model, we find that the room temperature carrier mobility reaches 7,000 cm^2/Vs, the highest mobility recorded for graphene in an aqueous electrolyte environment. Our results show that the electrical performance of SiO_2-supported graphene is robust, even in the presence of dissolved ions that introduce additional mechanisms for Coulomb scattering.

Key words: Biotransistor, biosensor, field-effect transistor

Electrolyte-gated graphene is used for electronic biosensing applications,[1] supercapacitor applications,[2] and fundamental measurements of graphene properties at high carrier concentration.[3] The electrolyte environment likely affects the mobility of charge carriers in graphene. Of particular concern is the case of graphene biosensors (typically operated in aqueous electrolyte), for which carrier mobility is critical to device performance.

A significant effort has been made to optimize the carrier mobility in dry graphene devices that are supported by a silicon oxide substrate. Benchmark mobility values for graphene derived from chemical vapor deposition (CVD) are ~ 7,000 cm^2/Vs,[4] and slightly higher values are sometimes found with mechanically exfoliated graphene (~ 10,000 cm^2/Vs).[5] When an SiO_2-supported graphene device is placed into an aqueous electrolyte, however, we lack clear expectations for the carrier mobility, as the presence of salt ions in the liquid introduces a new mechanism for Coulomb scattering. Previous work related to this question was performed by Newaz et al., who investigated the effect of salted, non-aqueous liquids on the carrier mobility of suspended graphene devices.[6] Additional insight comes from transconductance measurements of graphene field effect transistors (FETs) contacted by two probes and gated by aqueous electrolyte.[7,8,9,10,11] For example, Hess et al. used FET measurements of two-point conductance as a function of liquid gate voltage to estimate the relationship between sheet conductivity, σ_s, and sheet carrier density, n_s.[11] Surprisingly, there have been no direct measurements of σ_s as a

function of n_s for graphene gated by an aqueous electrolyte, and therefore no direct measurement of carrier mobility, μ, in this system.

Measuring carrier mobility in electrolyte-gated graphene is more challenging than the equivalent measurement of dry, back-gated graphene. First, n_s is not simply the product of the gate voltage and a constant gate capacitance. The gate capacitance changes with gate voltage due to quantum capacitance effects.[12] Moreover, the double-layer capacitance between the electrolyte-graphene interface has not been well established. Second, if the electrolyte environment contacts the metal electrodes, the electrolyte gate interferes with the voltage measurements that are required to establish n_s and σ_s.

In this work, we overcome the challenges of measuring carrier mobility in aqueous electrolyte. Graphene electrodes are capped with an insulating layer of SiO_2 to minimize the interference between the electrolyte gate and the voltage measurements. The Hall effect is used to measure sheet carrier density as a function of electrolyte gate voltage. We find a peak carrier mobility greater than 7000 cm^2/Vs, comparable to the benchmark values for dry graphene on SiO_2.

Graphene on copper foil was produced in our chemical vapor deposition system. Copper foil (25 μm thickness, Alfa Aesar) was cleaned with dilute nitric acid (5%) followed by acetic acid.[13] The foil was annealed for 60 min in H_2 gas at 1070°C, before starting graphene deposition (30 min at 1070°C, 20 sccm H_2, 30 sccm CH_4, pressure 50 Pa).[14] A wet transfer process was used to place the graphene on an Si/SiO_2 substrate (300 nm thermally-grown oxide).[15] The graphene was patterned using a two-layer photolithography process (Shipley S1813 photoresist over a base layer of MicroChem LOR) and O_2 plasma. A second photolithography step was used to create metal electrodes

encapsulated by SiO_2 (5 nm Cr, 30 nm Au, 70 nm SiO2). The electrode materials were deposited via e-beam evaporation. After device fabrication the graphene was characterized using microRaman spectroscopy (see supplementary material). Figure 1 shows a completed device, in which $L = w = 40$ μm.

All experiments were performed with the graphene device submerged in an NaCl aqueous solution (100 mM) with phosphate buffer (10 mM) to stabilize the pH at 7.2. The electrostatic potential of the liquid gate, V_{lg}, was controlled using a tungsten wire immersed in the electrolyte (see Fig. S2 in the Supporting Information). A current source (Keithley 2400 Source meter) was used to supply a dc current, $I = 5$ μA. The magnetic field, B, was applied perpendicular to the graphene using a variable-field electromagnet (+/- 0.5 T). Gate voltage sweeps were performed at a rate of 10 mV/s.

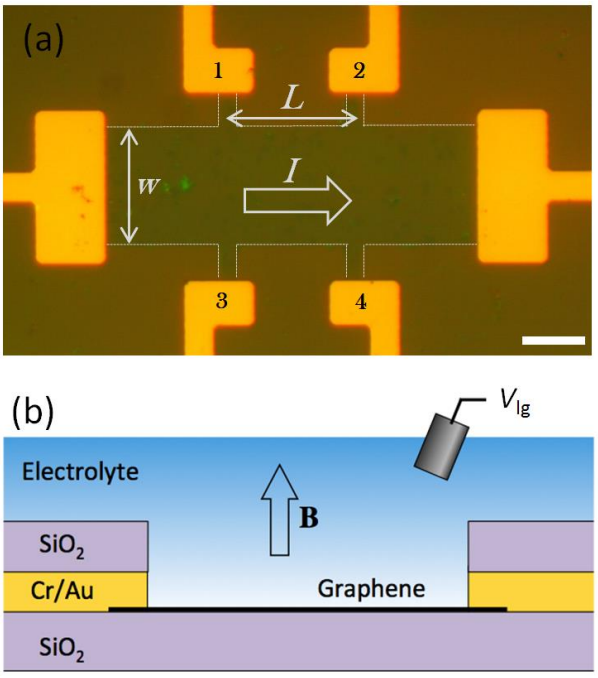

FIG. 1. Device geometry. (a) Hall bar geometry with constant current applied as indicated. Dashed white lines show the edge of the patterned graphene. The numbered electrodes are

used to measure voltage differences; for example, V_{13} is the voltage difference between electrodes 1 and 3. Scale bar 20 μm. (b) Cross-sectional diagram of the device. The Cr/Au contacts are capped in SiO_2. The magnetic field is perpendicular to the graphene.

Figure 2 shows the Hall voltage, V_H, measured when $B = \pm 0.5$ T. The measurement procedure is as follows. First, V_{13} is measured at $B = 0$ to establish the gate-dependent background voltage. This background voltage (of the order 0.1 mV) is related to the spatial inhomogeneity in the electrolyte gate potential. Next, V_{13} is measured at $B = \pm 0.5$ T. The Hall voltage is then $V_H = V_{13}(B = \pm 0.5\ \text{T}) - V_{13}(B = 0)$.

When $B > 0$ (red line), V_H is positive for hole-type transport and negative for electron transport. When $B < 0$ (black), the sign of V_H reverses. The transition from hole transport to electron transport occurs at the Dirac point, $V_D \sim 0.03$ V with respect to the tungsten electrode.

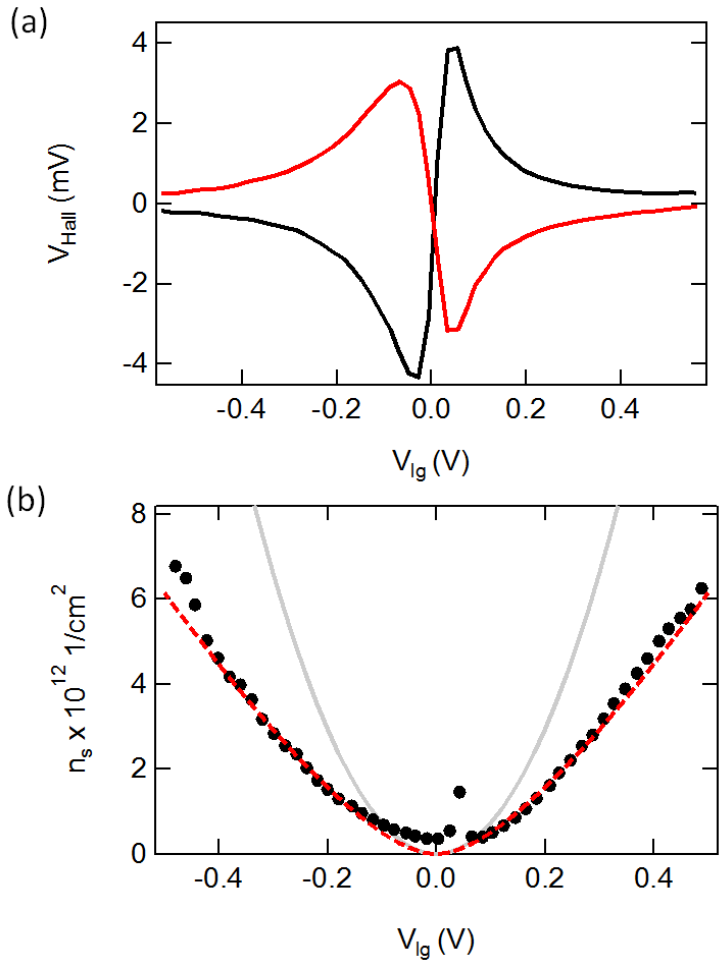

FIG. 2. Hall-effect measurements of electrolyte-gated graphene. The aqueous electrolyte is 100 mM NaCl. (a) The Hall voltage, V_H, measured when $B = \pm 0.5$ T. The raw V_{13} data (not shown) includes a gate-dependent background (~ 0.1 mV) that has been subtracted. b) Black dots represent the sheet carrier density, n_s, determined from V_H (Eq. 1). The grey line represents the calculated density when $C_{dl} >> C_q$ (the quantum capacitance limit). The red dashed line is calculated from Eq. 3 with $C_{dl} = 5$ μF/cm^2.

The sheet carrier density is inversely proportional to the Hall voltage,

$$n_s = \frac{BI}{V_H e}. \qquad (1)$$

We calculate n_s as a function of V_g using Eq. 1 (Fig 2b, black dots).

To understand the relationship between n_s and V_{lg} (Fig. 2b), we consider both the graphene density of states and the double-layer capacitance between the electrolyte gate and carriers in the graphene, C_{dl}. Assuming a tight binding model for the graphene dispersion relation, n_s scales as E_F^2, where E_F is the Fermi energy measured relative to the Dirac point.

$$n_s = \frac{1}{\pi}\left(\frac{E_F}{\hbar v_F}\right)^2, \qquad (2)$$

where the Fermi velocity is $v_F \sim 10^6$ ms^{-1}, and $\hbar$ is the reduced Plank constant. The quantum capacitance of graphene, $C_q = e^2(dn_s/dE_F)$, approaches zero as E_F approaches zero. If $C_{dl} >> C_q$, C_q limits n_s such that $n_s \approx (10^{14}\ \mathrm{cm^{-2}V^{-2}}) \cdot V_{lg}^2$ (grey line on Fig. 2b.).

To account for C_{dl}, we model the system as two capacitors in series. The sheet charge density on C_{dl} and C_q is equal, and the voltage across each capacitor adds to V_{lg}. n_s is found by solving

$$V_{lg} = \frac{\hbar v_F \sqrt{\pi n_s}}{e} + \frac{e n_s}{C_{dl}}. \qquad (3)$$

Equation 3 fits our experimental data when $C_{dl} = 5\ \mu$F/cm^2 (red dashed line). The value of C_{dl} that we determine from fitting our measurements is consistent with a model developed by Dankerl et al. for the spatial charge and electrostatic potential distributions at a graphene/electrolyte interface.[16] The measured n_s values deviate from eq. 3 at small V_{lg}. In this low-doping regime, n_s is dominated by electrostatic disorder in the graphene. We find a disorder-induced carrier concentration, $n_{s,disorder} \sim 0.4 \times 10^{12}$ cm^{-2}, which is typical for SiO_2-supported graphene.[17]

After establishing $n_s(V_{lg})$, we turn to the sheet conductivity, $\sigma_s(V_{lg})$. Figure 3a shows the sheet conductivity, $\sigma_s = I/V_{12}$, which is calculated from the voltage drop V_{12} (see Fig. 1). The sheet conductivity is smallest at the Dirac point, V_D, and increases almost linearly with $|V_{lg} - V_D|$. The linearity of $\sigma_s(V_{lg})$ is described well by a Boltzmann transport model (red dashed line), as discussed further below. The transconductance, $d\sigma_s/dV_{lg}$, is a useful figure of merit for biosensor sensitivity. We observe a peak transconductance of 4.5 mS/V. This is higher than previous reports for graphene in an aqueous environment, and is indicative of high mobility.

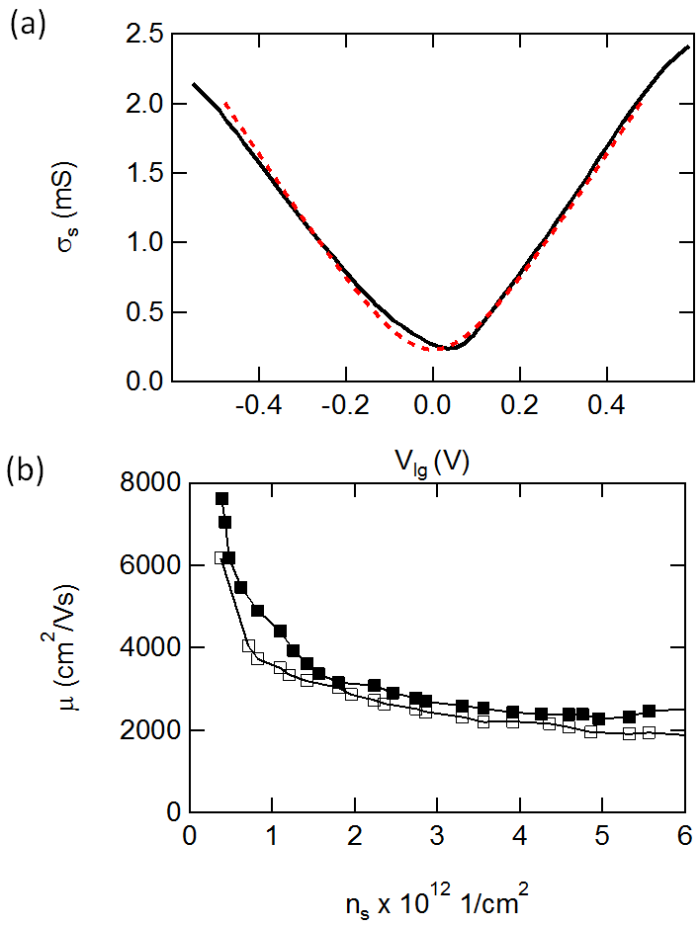

FIG. 3 Sheet conductivity and mobility measurements of electrolyte-gated graphene. The aqueous electrolyte is 100 mM NaCl. (a) The sheet conductivity as a function of V_{lg} (black line). Theoretical curve (dashed red line) based on Boltzmann transport theory with τv_F = 70 nm. (b) The Drude carrier mobility for electrons (solid squares) and holes (open squares).

The commonly-used framework for interpreting σ_s is the Drude model: $\sigma_s = \mu e n_s$, where μ is the Drude mobility. Figure 3b shows the calculated μ values for electrons and holes based on the measurements of n_s and σ_s. The maximum mobility exceeds 7,000 cm^2/Vs, matching the typical benchmark for dry GFET devices on SiO_2 substrates.

Our measurements of σ_s and μ (Fig. 3) give insight into the effect of aqueous electrolyte on graphene's electronic properties. The mobility-limiting factor in graphene is thought to be Coulomb scattering caused by charged impurities.[18] There are at least two roles that aqueous electrolyte could play in Coulomb scattering. First, dissolved ions could act as charged impurities, thereby decreasing μ. Second, the dielectric constant of the water may screen charged impurities, thereby increasing μ. The effectiveness of dielectric screening would depend on the location of the charged impurities. For example, dielectric liquid above the graphene cannot effectively screen charge traps located in the SiO_2 underneath the graphene.

We tested the possibility that dissolved ions reduce μ by measuring μ in a variety of salt concentrations. Figure S3 (Supporting Information) shows that μ is unchanged by varying salt concentration from 1 mM to 100 mM. To explore the second possibility (dielectric screening increases μ), we compare our measurements to previous work on dry, SiO_2-supported CVD graphene in which $\mu \sim 7{,}000$ cm^2/Vs.[4] Since we find a similar μ for our water-gated, SiO_2-supported graphene, we postulate that charge traps buried in the SiO_2 substrate are likely the limiting factor in both a dry environment and an aqueous electrolyte environment.

A recent experiment by Newaz et al.[6] corroborates our claim that the SiO_2 substrate has much greater effect on μ than the salt ions in the aqueous electrolyte. Newaz et al. investigated the effect of submerging suspended graphene devices in a non-aqueous solution (anisole) with dissolved salt (tetrabutylammonium tetraphenylborate). In a low-salt solution, mobility was enhanced due to the dielectric screening properties of anisole. Increasing the salt concentration from 0.01 mM to 100 mM reduced μ from

50,000 cm^2/Vs to 20,000 cm^2/Vs. A mobility of 20,000 cm^2/Vs is significantly higher than μ in SiO_2-supported graphene. Therefore, Newaz's result suggests that our measurement of μ ~ 7,000 cm^2/Vs is more likely attributable to the SiO_2 substrate than to dissolved salt ions.

Figure 3a includes a fitting curve based on Boltzmann transport theory. Unlike the Drude model, the Boltzmann transport model accounts for the Pauli-exclusion principle and the distribution of electrons in k-space. For a 2d material with relativistic dispersion, Boltzmann transport theory predicts,[18]

$$\sigma_s = \frac{2e^2}{h}\tau v_F\sqrt{\pi n_s}, \qquad (4)$$

where τ is the energy-averaged carrier scattering time. Combining equations 3 and 4 yields a good fit to the measured data when τv_F = 70 ± 5 nm (dashed line Figure 3a).

It is interesting that Boltzmann transport describes the sheet conductivity with a single fit parameter, τv_F, in contrast to the Drude model, which is fit by allowing μ to change as a function of n_s. Previous reports of graphene's electronic properties have favored the Drude model over the Boltzmann transport model (eq. 4), perhaps because τ varies with n_s for dry graphene devices.[19] However, it appears that τ is insensitive to n_s when screening is provided by a dielectric fluid. In future work, it will be interesting to explore the application of the Boltzmann transport theory for electrolyte-gated graphene.

In conclusion, we have measured the carrier mobility for graphene submerged in an aqueous electrolyte. The measured room-temperature mobility is significantly higher than traditional semiconductors such as silicon, and is comparable to benchmark values reported for dry graphene on SiO_2 substrates. This is the first time that the robustness of graphene's superb electrical properties has been demonstrated in an aqueous electrolyte

environment. Future experiments on suspended graphene, or graphene on hexagonal boron nitride, may demonstrate even higher mobilities in aqueous electrolyte. Graphene's high carrier mobility in aqueous electrolytes, together with mechanical strength/flexibility, chemical stability, and biocompatibility, suggests an exciting future for graphene biosensor applications.

Supporting Information

Characterization of graphene quality. Chip carrier design and the liquid-gate electrode. Relationship between salt concentration and graphene carrier mobility.

Acknowledgements

Funding for this research was provided by the National Science Foundation under award number DBI-1450967. M.R.L. and Y.B.Q. would like to thank funding from the Energy Materials and Surface Sciences Unit of the Okinawa Institute of Science and Technology Graduate University to support the synthesis of graphene samples, which was performed at OIST. We thank Michael Reynolds and Paul McEuen for valuable discussions. Device fabrication was performed at the MaSC Facility at Oregon State University.

Bibliography:

[1] Y. Liu, X. Dong, and P. Chen, Chem. Soc. Rev. **41**, 2283 (2012).

[2] K.S. Novoselov, V.I. Fal'ko, L. Colombo, P.R. Gellert, M.G. Schwab, and K. Kim, Nature **490**, 192 (2012).

[3] J. Ye, M.F. Craciun, M. Koshino, S. Russo, S. Inoue, H. Yuan, H. Shimotani, A.F. Morpurgo, and Y. Iwasa, Proc. Natl. Acad. Sci. U. S. A. **108**, 13002 (2011).

[4] J. Chan, A. Venugopal, A. Pirkle, S. McDonnell, D. Hinojos, C.W. Magnuson, R.S. Ruoff, L. Colombo, R.M. Wallace, and E. Vogel, ACS Nano **6**, 3224 (2012).

[5] L.A. Ponomarenko, R. Yang, T.M. Mohiuddin, M.I. Katsnelson, K.S. Novoselov, S. V. Morozov, A.A. Zhukov, F. Schedin, E.W. Hill, and A.K. Geim, Phys. Rev. Lett. **102**, 100 (2009).

[6] A.K.M. Newaz, Y.S. Puzyrev, B. Wang, S.T. Pantelides, and K.I. Bolotin, Nat. Commun. **3**, 734 (2012).

[7] G. Saltzgaber, P. Wojcik, T. Sharf, M.R. Leyden, J.L. Wardini, C.A. Heist, A.A. Adenuga, V.T. Remcho, and E.D. Minot, Nanotechnology **24**, 355502 (2013).

[8] Z. Cheng, Q. Li, Z. Li, Q. Zhou, and Y. Fang, Nano Lett. **10**, 1864 (2010).

[9] I. Heller, S. Chatoor, J. Männik, M.A.G. Zevenbergen, C. Dekker, and S.G. Lemay, J. Am. Chem. Soc. **132**, 17149 (2010).

[10] Y. Ohno, K. Maehashi, Y. Yamashiro, and K. Matsumoto, Nano Lett. **9**, 3318 (2009).

[11] L.H. Hess, M. V. Hauf, M. Seifert, F. Speck, T. Seyller, M. Stutzmann, I.D. Sharp, and J.A. Garrido, Appl. Phys. Lett. **99**, 033503 (2011).

[12] J. Xia, F. Chen, J. Li, and N. Tao, Nat. Nanotechnol. **4**, 505 (2009).

[13] S.M. Kim, A. Hsu, Y.-H. Lee, M. Dresselhaus, T. Palacios, K.K. Kim, and J. Kong,

Nanotechnology **24**, 365602 (2013).

[14] H. Zhou, W.J. Yu, L. Liu, R. Cheng, Y. Chen, X. Huang, Y. Liu, Y. Wang, Y. Huang, and X. Duan, Nat. Commun. **4**, 2096 (2013).

[15] M.A. Brown, L. Barker, L. Semprini, and E.D. Minot, Environ. Sci. Technol. Lett. **2**, 118 (2015).

[16] M. Dankerl, M. V. Hauf, A. Lippert, L.H. Hess, S. Birner, I.D. Sharp, A. Mahmood, P. Mallet, J.Y. Veuillen, M. Stutzmann, and J.A. Garrido, Adv. Funct. Mater. **20**, 3117 (2010).

[17] S. Adam, E.H. Hwang, V.M. Galitski, and S. Das Sarma, Proc. Natl. Acad. Sci. U. S. A. **104**, 18392 (2007).

[18] S. Das Sarma, S. Adam, E.H. Hwang, and E. Rossi, Rev. Mod. Phys. **83**, 407 (2011).

[19] E. Hwang, S. Adam, and S. Sarma, Phys. Rev. Lett. **98**, 186806 (2007).